A few remarks on the kinetics of grain growth in rocks

3 **AUTHORS**, INCLUDING:

Brian Evans
Massachusetts Institute of Technology
113 PUBLICATIONS **4,812** CITATIONS

SEE PROFILE

Jane Dagmar Pollo Renner
University of Santa Cruz do Sul
76 PUBLICATIONS **894** CITATIONS

SEE PROFILE

ORIGINAL PAPER

B. Evans · J. Renner · G. Hirth

A few remarks on the kinetics of static grain growth in rocks

Abstract Static grain growth is a relatively simple transformation in which grain size increases under driving forces caused by grain and interphase boundary curvature. Given the relative simplicity of the protocol for grain growth experiments, measurements of grain boundary mobility show surprising variations. Boundary mobilities during grain growth are affected by solute and impurity chemistry, chemical fugacity of trace and major elements, pore size and number, pore fluid chemistry, the presence of melts, and the presence of solid second phases, as well as temperature and pressure. All of these factors may exert influence on grain growth of rocks in natural situations and many are also present during the laboratory experiments. Provided that the necessary kinetics parameters are known, bounds may be placed on the interface mobility when pores, partial melts, or solutes are present. To predict the rate of grain growth in natural situations will require improved laboratory data and careful consideration of the thermodynamic conditions likely to be encountered in nature.

Keywords Grain growth · Ostwald ripening · Pore drag · Recrystallization

B. Evans (✉)
Department of Earth, Atmospheric, and Planetary Sciences,
Massachusetts Institute of Technology, Cambridge,
MA 02139, USA
E-mail: brievans@mit.edu
Phone: +1-617-2532856
Fax: +1-617-2580620

J. Renner
Department of Earth, Atmospheric, and Planetary Sciences,
Massachusetts Institute of Technology, Cambridge,
MA 02139, USA

G. Hirth
Geology and Geophysics, Woods Hole Institution,
Woods Hole, MA 02543-1541, USA

List of symbols

$\aleph_v$	area of boundaries per unit volume consumed by another boundary
A_b	area of migrating boundary
$C,\ C'$	constants relating boundary curvature to grain size, ~1–5
$C^{(m)}$	constant relating maximum grain size to d_p/f (model dependent)
D_{gb}	grain boundary diffusion coefficient
D_0^{mech}	pre-exponential kinetics factor, depends on transport path and mechanism
δ	grain boundary width
d_p	particle size of second phase
E_p	ellipticity of second phase particle
f_{vol}	volume fraction of second phase
f_i	fugacity of component IF driving force for grain growth
F_{discon}	driving force for discontinuous grain growth
F_n	net force on an individual boundary
F_p	drag force exerted by a pore or particle
F_{Zener}	drag force owing to second phase particle when boundary is pinned
G_{b1}, G_{b2}	individual migrating boundaries
$\overline{g}, \overline{g}_0$	average grain size at time, t or $t_0 g$ grain size of individual grain at time, $t g_c$ critical grain size for a distribution of grains
g_{sph}	spherical grain size ΔG incremental change in Gibbs free energy
γ	interface specific Gibbs free energy

γ_{ave}	specific interface energy averaged over all orientations
θ	angle between pinned boundary and boundary if it were unpinned
k_{BZ}	Boltzmann's constant
K_{og}	pre-exponential constant for grain-growth, a function of chemical fugacity
κ_{og}	empirical grain-growth kinetics constant, where $K_{og} = \kappa_{og} f_i^m$
K_{int}	intrinsic kinetic coefficient ($= 2CM_{int}\gamma$)
L_3	mean intercept length determined by stereology
M_{ave}	average boundary mobility
M_{int}	intrinsic (individual) boundary mobility
M_b	individual boundary mobility
M_p	individual pore or particle mobility
n	power law constant for grain growth, $2<n<6$
m	power law constant for mobility of pore, mechanism dependent
r_1, r_2	principal radii of curvature of interface
Q_g	empirical activation energy for grain growth rate constant
Q^{mech}	activation enthalpy for rate-limiting transport mechanism
R_p	radius of a second phase particle
t	time
t_0	starting time
T	temperature
Vol_{swept}	crystal volume swept by migrating boundary
V_b	velocity of individual boundary
V_p	particle or pore mobility
Ψ	dihedral angle between two interfaces
Ω	volume of unit cell
$\eth$	thickness of melt film

Introduction

Grain growth and recrystallization are part of a class of microstructural transformations that have profound implications for the texture of rocks (Urai et al. 1986), for strength of rocks during diffusion creep (Hirth and Kohlstedt 1995; Karato 1984; Karato et al. 1986; Hirth and Kohlstedt 1995), and for brittle fracture strength (Olsson 1990). The kinetics of grain growth can be used to infer thermal history around contact aureoles (Joesten 1991). Changes in grain size could also profoundly affect the physical properties of rocks in the lower crust and upper mantle. For example, in partially molten rocks, if the melt topology achieves homogeneous textural equilibrium, then the permeability of the solid phase will be related to grain size and the abundance of the melt (Kohlstedt 1992). Grain boundary migration can be combined with reactions to provide coupled textural and geochemical variations (Yigang et al. 1998). Watson et al. (1989) have pointed out that the assumption that accessory phases fully participate in anatexis requires those phases to

be in chemical contact with the melt as it develops. Thus, to remain in chemical contact, the accessory phases must reside on or near a high diffusivity pathway (e.g., the connected melt porosity or a high-diffusivity grain boundary). If fast boundary migration were possible, the accessory phases (or a melt pocket) might be included within a grain, effectively removing it from interaction with the connected melt phase. In this brief tutorial note, we discuss some of the variables that affect grain growth kinetics. Even in closely controlled laboratory experiments, the growth kinetics may be quite complicated and unconstrained. We argue that much more data are needed to predict growth rates in nature accurately.

Recrystallization and grain growth in rocks

Recrystallization in solid and partially molten rocks may be driven by chemical reactions (chemically induced grain boundary migration), by reduction of stored energy associated with defects (static or primary recrystallization), or by reduction of boundary energy (grain growth; Drury and Urai 1990; Urai et al. 1986). The magnitudes of the driving forces vary according to the exact situation, but for most natural cases, reaction forces tend to be greatest, defect energy intermediate, and boundary reduction forces least (Urai et al. 1986). More important than the magnitude of the driving force are the actual migration rates, i.e., the product of boundary mobility and driving force. Qualitative comparisons of transport distances and boundary migration rates may be used to map kinetic transport regimes (Cahn and Balluffi 1981; see also Evans et al. 1986). Although forces from reduction of boundary energy tend to be lowest, unlike the other two forces, they are always present in a polycrystalline rock, and thus, grain growth is likely a common process.

Static grain growth may be further divided into normal or abnormal growth. During normal grain growth, the average grain size increases, while a narrow distribution of both grain size and shape is maintained (Atkinson 1988). That process may be contrasted with abnormal grain growth, during which a few large grains develop and grow, consuming smaller, more numerous, matrix grains.

Laboratory experiments to investigate grain growth are often rather simple: a small sample is inserted into a furnace with or without additional confining pressure and heat-treated for various periods. The sample is retrieved and the grain size measured by observation in thin section or by using a scanning electron microscope. Valuable information has been gained by direct optical observation of the process (Means and Park 1994; Fig. 1). Normal grain growth during the experiment can be characterized by the time evolution of the average grain size, because the form of the distribution of grain sizes is constant.
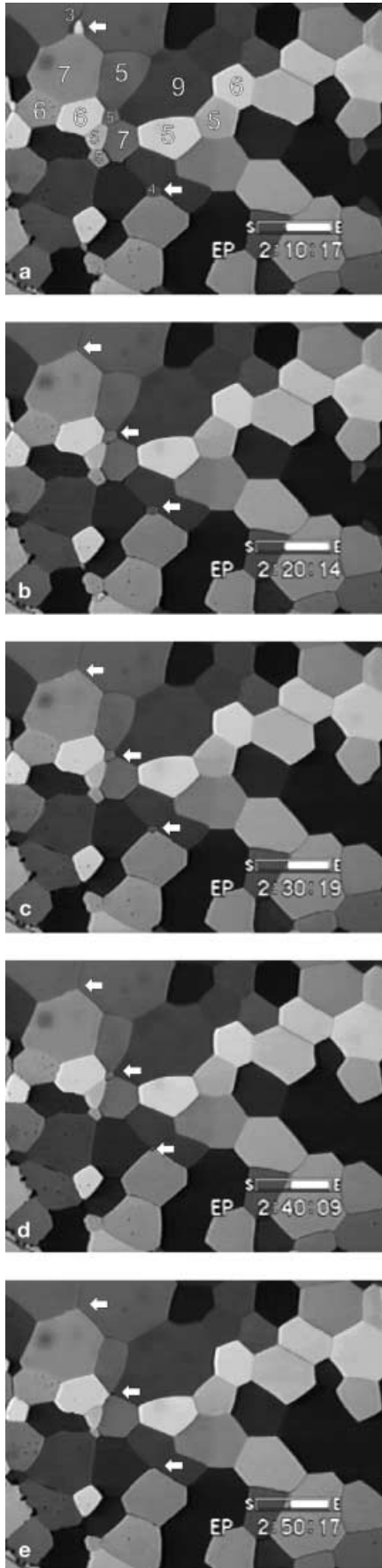
The average grain size, $\bar{g}$, of the matrix during laboratory experiments with minerals, ceramics, and metals, is often found to increase with time according to the relation

$$\bar{g}^n - \bar{g}_0^n = K_g \cdot t \tag{1}$$

where $\bar{g}_0$ is the average grain size at time t_0, n is a constant of order 2–5, t is the elapsed time. K_g is a thermally activated rate constant (Atkinson 1988):

$$K_g = K_{og} \exp -\left(Q_g/RT\right) \tag{2}$$

In some cases, K_g can be related to a boundary diffusion coefficient, and, thus, K_{og} may be a function of the fugacity of the i components of the mineral, f_i, such that

$$K_{og} = \kappa_{og} \prod_i f_i^{m_i} \tag{2b}$$

where κ_{og} is a constant, and m_i may be either positive or negative (Nichols and Mackwell 1991).

Shown in Fig. 2 and Table 1 are results from several laboratory investigations of grain growth in peridotite rocks (references are given in Table 1). Given the relative simplicity of the experimental protocol, the scatter in the data from one suite of experiments to another is quite striking. Although experimental errors are inevitable, it can be argued that the observed variations in rate are real and are caused by variations in sample chemistry, fluid-inclusion content, melt chemistry, melt content, dissolved impurities, or solid accessory phases. All these influences are possible in natural situations. In general, grain growth in peridotites is slowest in experiments done at dry conditions, without melt, at low confining pressure, and where gas-filled porosity is present. Growth is intermediate when samples are partially molten, in dry conditions, and at room pressure. Grains grow fastest when water is added at higher confining pressure.

To use the kinetics equations [(Eqs. (1) and (2)] to predict grain growth in natural situations, one needs to understand the physics behind them. Equation (1) results from determining the response of the grain boundaries to the driving force for grain growth, i.e., reduction of total interfacial energy. The ability for a particular grain boundary to move, per unit driving force, is called the boundary mobility, M_b. What
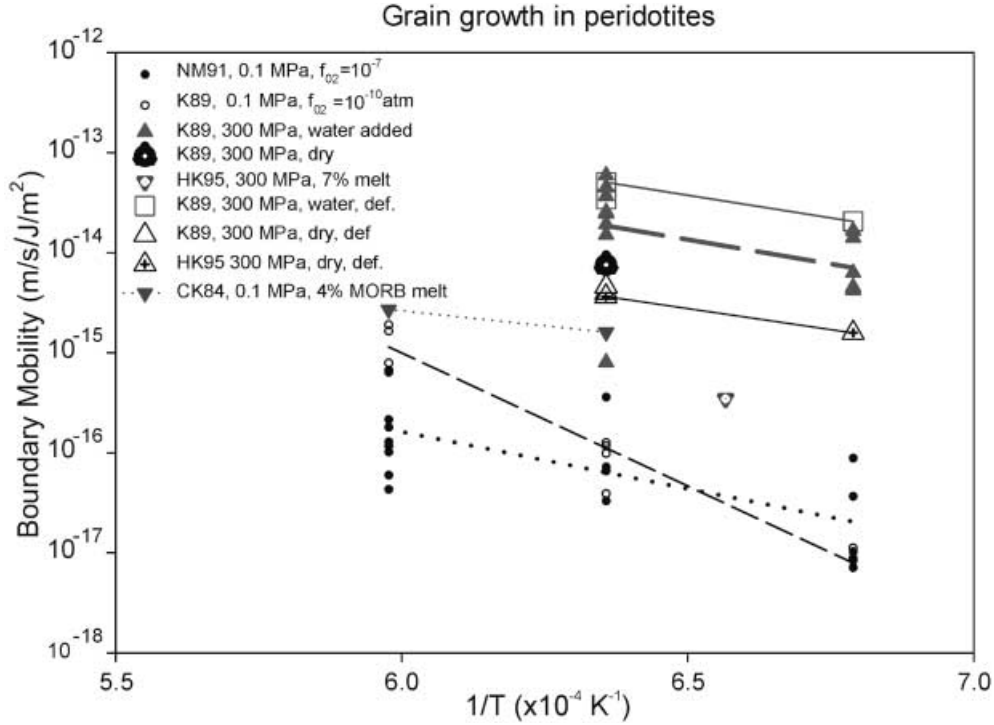
Grain growth in peridotites

Fig. 2 Grain boundary mobility $[(m/s)\cdot(m^2/J)]$ as a function of $1/T$ (K^{-1}) for peridotites. Mobility may be estimated from normal grain growth data using Eq. (9) and from abnormal grain growth using Eq. (7), assuming that $\gamma=1$ J/m^2. Notice that the data span about four orders of magnitude in mobility at a given temperature. Samples deformed with no added water and without melt at room pressure (0.1 MPa) grow most slowly. Dry, partially molten peridotites with and without elevated confining pressure have intermediate mobilities, whereas dry samples with no melt treated with elevated temperature and pressure have slightly higher mobilities. Grain growth is fastest in samples with added water and elevated pressure. Grain growth during diffusion creep occurs at roughly the same rate as static grain growth. *CK84* (Cooper and Kohlstedt 1984); *NM91* (Nichols and Mackwell 1991); *K89* (Karato 1989b); *HK95* (Hirth and Kohlstedt 1995)

determines boundary mobility? How is it related to the kinetics of Eq. (1)? In the kinetics equation, what determines the value of n? How does the rate constant vary with temperature? What effects do dissolved impurities, solid phases, or fluids, such as gas or water, have on the rate of growth in rocks? Under geological conditions, what constraints may be placed on the effect of these influences and which are likely to be most important?

Driving forces and boundary mobility

The driving force for grain growth is the reduction of Gibbs free energy (ΔG) per unit motion of a unit area of grain boundary. Migration forces can be exerted by reduction in interfacial area of the moving boundary

itself, by torque forces exerted by the motion of neighboring boundaries, or by destruction of surrounding boundaries (Fig. 3; Yan et al. 1977; Powers and Glaeser 1998; Yan et al. 1977). When the motion of a boundary is driven by reduction of its own curvature (and hence, reduction in total interfacial area) then the driving force, F, is

$$F = -\gamma\left(\frac{1}{r_1}+\frac{1}{r_2}\right) \tag{3}$$

where γ is the specific energy of the boundary or interface that is being removed, and r_1 and r_2 are the principal radii of curvature at a given instant (i.e., the mean normal curvature is the sum of the two principal curvatures).

Part of the difficulty in providing an explicit kinetics law for grain growth in actual materials arises from accurately relating the local curvatures to the average grain size (Atkinson 1988). In real materials, a range of grain sizes exists, and topology suggests that those grains smaller than a critical size, g_c, will have highly curved convex boundaries and will therefore shrink. Hillert (1965) suggested that the net driving force, F_n, on a particular boundary may be approximated as

$$F_n = 2C\gamma\left(\frac{1}{g_c}-\frac{1}{g}\right) \tag{4}$$

where g is the size measure of the grain being considered, and C is a factor that relates the boundary curvature to g; C is a number that depends on the details of the grain geometry and size. During normal grain growth, C is ~1 when $g<<g_c$ According to Hillert's (1965) treatment, the average grain size

Table 1 Some laboratory determination of grain growth kinetics in calcite and peridotite aggregates

Material	T (K)	n	Q (kJ/mol)	κ_o (m^n/s)	Remarks	Reference
Calcite (Solnhofen)	650	3			Ostwald ripening in fluid	Chai (1974) Chai (1974)
	600–1000	2.5–7	190		Oven dried	Schmid et al. (1977)
	650–1000	2.5–5	200		Dry and wet	Tullis and Yund (1982)
	700–800	2.2	131		Water added	Rutter (1984)
	700–800	>5			Water added	Olgaard and Evans (1988)
Carrara (Synthetic)	1200	5.6			Oven dried	Olgaard (1990)
	650–800	3	174	2.5×10^{-9a}	Water added; melt present	Covey-Crump (1986)
	700–800	2.6–4	180±50		Dry and wet	Olgaard and Evans (1988)
	500–1200	3	172±60		Oven dried	Olgaard (1990)
	700–800	3	232	1×10^{-7a}	Pure samples with/with out fluids	Covey-Crump (1997)
	550–700	3	162	6×10^{-11a}	Fluid-added; pressure dependence of Q	
	550–700	4–9			Dry	
	973–1173	2	99	3×10^{-10a}	10 ppm Mn; P_c=300 MPa; dry	D. Freund and G. Dresen (personal communication, 2000)
		2.4	160	5×10^{-8a}	350 ppm Mn; P_c=300 MPa; dry	
		2.2	147	5×10^{-8a}	660 ppm Mn; P_c=300 MPa; dry	
Peridotite (Syn.)	1473–1673	4	290±20	8.1×10^{-16}	$K_{og} = 7.4 \cdot 10^{-16} \cdot f_{O_2}^{0.13}$	Nichols and Mackwell (1991)
		5	345±25	7.4×10^{-19}	$K_{og} = 7.4 \cdot 10^{-16} \cdot f_{O_2}^{0.13}$ P_c=0.1 MPa, swelling $\log f_{O_2} = -4$ to -11 (atmosphere)	
	1473–1673	2	520	5×10^{-8a}	P_c=0.1 MPa, swelling	Karato (1989a)
		3	600		$\log f_{O_2} = -10$ (atmosphere)	
	1473–1573	2	160	1.6×10^{-8a}	P_c=300 MPa, wet	
		(2)	(160)	5×10^{-8a}		Hirth and Kohlstedt (1995)

^{a} No fugacity dependence is given or known, and therefore, $K_{og}=\kappa_{og}$

$$\bar{g} \approx \frac{8}{9} g_c \qquad (5)$$

From Eq. (4), we see that grains smaller than g_c shrink, whereas those larger than g_c grow.

If some grains are initially much larger than g_c, boundary migration of the large grain will be driven by the reduction of area of adjoining boundaries being swept by the moving boundary, a situation variously called abnormal (Atkinson 1988), discontinuous (Chiang et al. 1997; Stöckhert and Duyster 1999) or secondary grain growth. See Fig. 3c for an illustration. We use abnormal and discontinuous synonymously. As the migrating boundary sweeps through a volume, Vol_{swept}, containing other interfaces of total area, $\aleph$, the driving force per unit area of migrating boundary, is

$$F = -\frac{1}{A_b}\frac{d\Delta G}{dx} = \frac{1}{A_b}\left(-\frac{d\Delta G}{d\aleph}\right)\left(\frac{d\aleph}{dVol_{swept}}\right)\left(\frac{dVol_{swept}}{dx}\right)$$
$$= -\gamma \cdot \aleph_v \qquad (6)$$

where $dVol_{swept}/dx$ is A_b, the area of the sweeping boundary, $\aleph_v$ is the interfacial area of other boundaries being removed as a unit volume of crystal is swept by the migrating boundary (Yan et al. 1977; Powers and Glaeser 1998; Yan et al. 1977). The negative sign insures that the driving force is positive when the motion of the boundary causes the total interfacial area to be reduced. Notice that the units of

F are force per unit area, so F could also be called specific force or pressure, even though it results from chemical, and not mechanical, forces (Atkinson 1988).

The specific surface area is related to the mean intercept length, L_3, i.e., the average chord length of a randomly oriented line across a grain, by the relationship, $\aleph_v=2/L_3$ (Underwood 1970). The mean intercept length has the advantage that it is easily measured in plane section and that it does not require an explicit description of grain shape. For a boundary moving through a system of spherical grains, all with diameter, g_{sph}, the driving force becomes

$$F_{abnormal} = \frac{3\gamma}{g_{sph}} \qquad (7)$$

Notice that the total driving force is no longer determined by the curvature of the migrating boundary, but is related to the boundary energy of the grains being consumed. Thus, Hillert's factor, C, ranges from 1 to 1.5 depending on the size of the migrating grain relative to the critical size. It is important to realize that Eq. (1) does not accurately describe growth kinetics when abnormal growth occurs, because larger grains will be growing at rates that are unusually fast. Abnormal growth rates have been measured in partially molten peridotites at room pressure and 1573–1673 K by seeding large crystals in a finer-grained matrix (Cooper and Kohlstedt (1984); also see Fig. 2).
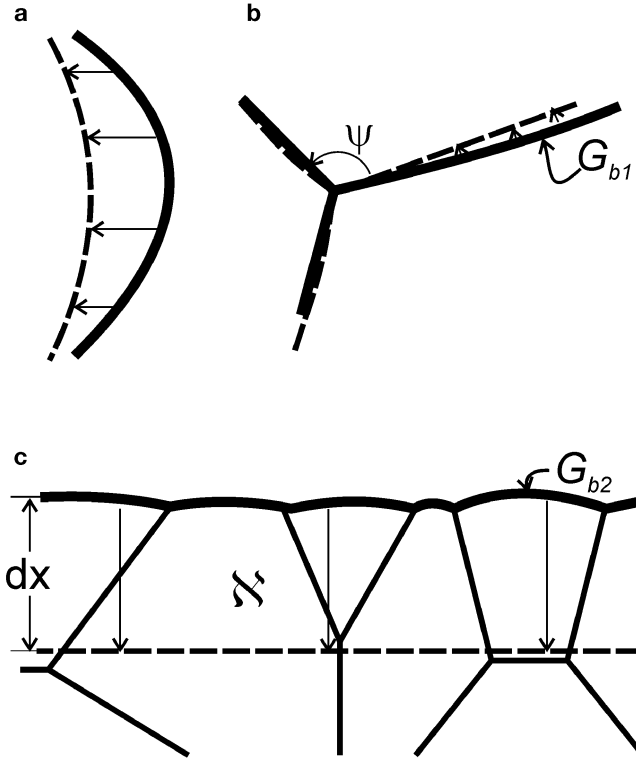
Fig. 3 Schematic of capillary-driven grain growth. **a** Growth driven by curvature reduction. **b** The vector balance of capillary forces at the intersection of three boundaries maintains a characteristic dihedral angle Ψ. If one boundary migrates, in this example, boundary, G_{b1}, the vector balance at the intersection may cause torque forces to be transmitted. **c** If very large grains exist within a fine-grained matrix, migration of the boundary of the large grain, G_{b2}, consumes smaller grains. The driving force for boundary migration is proportional to the boundary area of the consumed grains, $\aleph$

In all cases, the boundary velocity, V_b, is linearly related to the total driving force (per unit area of boundary), F_b, by the boundary mobility, M_b,

$$V_b = M_b F_b \tag{8}$$

The average boundary mobility may be estimated by assuming that the average boundary velocity equals half the average grain growth rate

$$V_b = \frac{1}{2} \frac{d\bar{g}}{dt}$$

and that the driving force is the average specific interfacial area divided by the average grain size, $\gamma_{ave}/\bar{g}$ [cf. Eq. (3)]. Then,

$$M_{ave} = \frac{1}{2} \cdot \frac{\bar{g}}{\gamma_{ave}} \cdot \frac{d\bar{g}}{dt} \tag{9}$$

Equation (9) provides a method of determining average mobility from aggregate grain growth data (Fig. 2). In general, both M_{ave} in Eq. (9) and γ in Eqs. (3), (4), (5), (6), (7), (8) and (9) may depend on

temperature, crystal orientation (Sutton and Balluffi 1995), major element chemistry, impurity content, and whether melt is present. If fluid inclusions or second phases exist, they, too, may exert forces on the boundary that will influence grain growth. Excepting variations caused by orientation, in the following we discuss the influence of each of these factors on the kinetics of grain growth, using olivine and calcite as examples pertinent to geology.

Parabolic growth kinetics

The classic treatment of grain growth (Burke and Turnbull 1952) assumes that boundary energy is isotropic and time-invariant, that boundary mobility is limited by self-diffusion of the crystal components across the boundary region, and that the only specific force (or pressure) on the boundary arises from boundary curvature. Then, the intrinsic boundary mobility is

$$M_{int} = \frac{\Omega D_{gb}}{\delta k_{BZ} T} \tag{10}$$

where D_{gb} is the grain boundary diffusion coefficient of the rate-controlling species for self-diffusion, Ω is the unit cell volume, δ is the boundary width, and $k_{BZ}T$, the usual Boltzmann factor. Notice that the intrinsic mobility is independent of curvature (or grain size). If the radius of curvature of the boundary is proportional to the grain diameter, g, and if the grain boundary velocity is proportional to the rate of change of the average grain size, by using Eq. (3), and inserting average values with constants to relate average grain size and curvature:

$$\frac{d\bar{g}}{dt} = C' M_{int} \frac{\gamma}{\bar{g}}$$

and

$$\bar{g}^2 - \bar{g}_0^2 = K_{int} t \tag{11}$$

where $\bar{g}_0$ is the grain size at time, $t=0$, and the rate constant $K_{int} = C' M_{int} \gamma$.

The mobility is termed intrinsic because it is limited solely by processes occurring along boundaries in a uniform matrix phase. Extrinsic controls on mobility may arise owing to impurity segregation, melt films, or interface reactions (Yan et al. 1977; Powers and Glaeser 1998; Yan et al. 1977). More localized extrinsic drag forces may result from fluid inclusions or solid phases that interact with the boundary as it migrates.

Effects of solutes and impurities

The concentration of solutes and impurities at the boundary may be elevated or depressed relative to the concentration in the bulk material. In ionic and cova-

Table 2 Growth kinetics – single phase

Mechanism	Limit	Boundary mobility	Exp.
Intrinsic	Self diff.	$M_{\mathrm{int}} = \frac{D_{\mathrm{b}}\Omega}{\delta kT}$	2
Liquid film	Liq. diff.	$M_{\mathrm{liq}} = \frac{D_{\mathrm{l}}C_{\mathrm{l}}\Omega}{\varpi kT}$	3
Interface limited	Int. react.	$M_{\mathrm{int}} = \frac{K\Omega}{k_{\mathrm{BZ}}T}$	2
Solute drag	Solute diff.	$M_{\mathrm{sol}} = \frac{D_{\mathrm{s}}\Omega}{2\delta kT(C_{\mathrm{s}}\mathrm{e}^{U/RT})}$	3

lent materials, such concentration variations arise from either elastic or electrostatic interactions between the impurity and the boundary. The inter-action energy of the concentration variations results in a coupling of boundary migration and impurity diffusion (Yan et al. 1977). As the boundary moves, the coupling exerts a drag force proportional to the velocity. In ceramic minerals such as Al_2O_3 and MgO, impurities at the level of several hundreds ppm may cause differences in grain boundary mobility of several orders in magnitude. The exact effect on boundary mobility depends on the details of the interaction potential between the impurities and the boundary, but in general, two regimes exist. At low velocities, solute drag dominates, resulting in extrinsically controlled boundary migration. In the extrinsic regime, boundary mobility is related to the concentration and diffusion rate of the solute, and the interaction potential. At higher velocities, the boundary may be able to outrun the solute and free itself from the drag force. As the boundary is released from the impurity drag force, unstable or jerky boundary motion may occur and manifest itself in wavy, bowed-out, boundary structures. A similar process occurs during dynamic recrystallization in salt (Guillope and Poirier 1979). In the extrinsic regime, conservation of the total amount of solute requires that impurity concentration at the boundary increases with grain size. Thus, the exponent, n, in Eq. (1) is 3 if impurity diffusion limits the mobility, and 2 in the high velocity limit, when mobility approaches the intrinsic limit (Table 2).

Notice also that, if a dissolved impurity is uniformly dispersed throughout the material, i.e., not segregated to the boundary, boundary migration is called intrinsic even though grain-boundary diffusion is affected by impurity content. This terminology leads to the confusing situation where intrinsic grain-boundary migration is limited by extrinsic diffusion processes. Depending on the effect of the impurity on diffusion rate, boundary mobility may be increased or decreased. For example, some impurities retard grain migration in Y_2O_3, but other dopants enhance it (Chen and Chen 1996). The enhancers seem to be undersized relative to the ion they replace, implying that the dopants migrate by some interstitial diffusion process along the boundary. Apparently point defect reactions involving these impurities can speed up diffusion of the species that is controlling the rate of grain growth.

Drag by discrete second phases

Rigid particles

When a second phase exists as a collection of discrete particles included within a polycrystalline matrix, the particles may retard, or even stop migration of the matrix grain boundaries, a process called Zener pinning (Nes et al. 1985). Indeed, fine-grained matrix grains are often associated with dispersed accessory minerals (Wilson 1973; Hobbs et al. 1976) both in dynamically and statically recrystallized rocks (Wilson 1973; Masuda et al. 1991). In addition to controlling the matrix grain size and exerting concomitant influence on the physical properties of the matrix, pinning affects the degree to which accessory minerals participate in metamorphic and anatectic reactions (Watson et al. 1989).

Zener pinning results from the change in energy when a migrating boundary encounters a particle of a second phase. The reduction in Gibbs free energy that occurs depends on the specific energy of the matrix/matrix interfaces and the area of the matrix boundary occluded by the particle (Nes et al. 1985). Provided that the boundary energy is not a function of the relative orientation of the grains on either side, i.e., the boundary energy is isotropic, then the energy reductions of the grain boundary/particle interactions are transmitted as capillary forces tangent to the boundary at every point. During normal grain growth in the matrix phase, if the migrating boundaries encounter a second-phase particle, boundary curvature forces are transmitted to the junction of the migrating boundary with the second phase particle (Fig. 4). If the particle is a rigid sphere, then the intersection of the matrix/matrix boundary and the matrix/particle boundary is a right angle. If the particle is deformable, e.g., a pore filled with a fluid in which the matrix is soluble, then the particle/pore will change its shape to balance capillary forces along the pore/matrix interface and along the matrix/matrix interface (Hsueh et al. 1982). Force balance at the junction of the matrix/matrix grain boundary and the pore/matrix interfaces will establish a dihedral angle that is determined by the ratio of the interfacial energies of the matrix/particle interface and the matrix/matrix energy (Blakely 1973).

When a migrating matrix/matrix boundary first approaches a second-phase particle, it will be attracted to it, i.e., boundary motion will tend to increase the occluded area (see Fig. 4b; Nes et al. 1985). If the boundary continues to migrate in response to capillary forces transmitted from the other grains, the occluded area will be maximum as the line between the points of intersection of the boundary with the particle become a diameter of the particle (rather than a chord). As the matrix/matrix boundary moves further through the particle, the particle exerts a drag force on the boundary, tending to retard boundary migra-
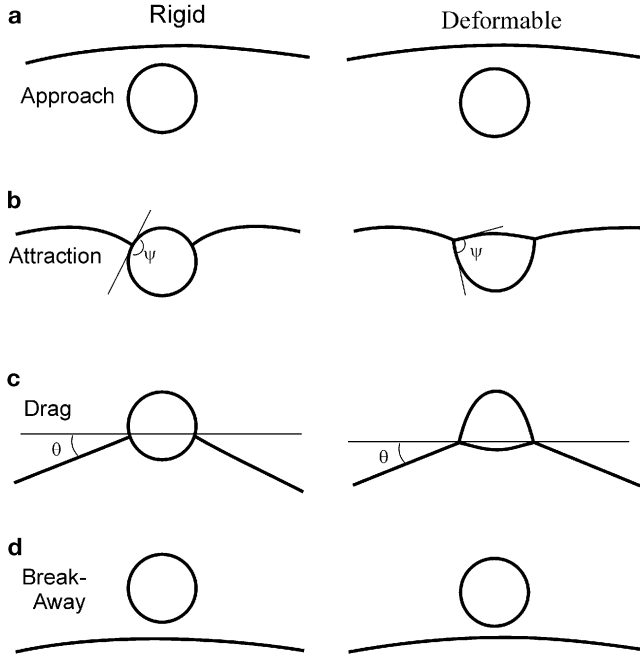
Fig. 4 Schematic of Zener pinning and pore drag. **a** Boundary approaches a rigid particle (left-hand series) and a deformable particle or pore (right-hand). **b** When the boundary initially encounters the particle/pore, it is attracted by virtue of the forces at the junction of the boundary and the particle. The dihedral angle at the rigid particle is maintained at 180°, whereas the dihedral angle, Ψ, at the pore boundary intersection is set by the ratio of the solid/solid boundary energy and the fluid/solid interfacial energy. **c** As the boundary continues to migrate the particle/pore begins to exert a pinning force that depends on the solid/solid grain boundary energy and the deformability of the particle. **d** If the capillary forces on the boundary exceed the pinning/drag force, then the boundary will break away from the particle/pore

tion (Fig. 4c). The force of interaction between the grain boundary and the particle may be sufficient to drag the particle along with the boundary providing that the mobilities of the ions composing the matrix and second phases are sufficiently large.

The pinning force exerted by an individual particle depends on the radius of the particle, on its shape, and whether the particle/matrix interface is coherent or incoherent (Table 3). For a rigid particle, the area of the particle/matrix boundary does not change. Thus, the pinning force depends only on the area occluded by the particle times the interfacial energy of the matrix/matrix boundary, γ (and not on the energy of the particle/matrix interface). For a rigid spherical, second-phase particle, the pinning force,

$$F_{\mathrm{Zener}} = \pi \gamma d_{\mathrm{p}} \cdot \cos\theta \cdot \sin\theta \qquad (12)$$

where d_{p} the radius of the second-phase particle, θ is the angle between the tangent to the pinned matrix boundary at its intersection with the particle and the tangent to the boundary if no particle were present (Fig. 4c). From Eq. (12), the maximum pinning force is $\pi\gamma d_{\mathrm{p}}/2$. The pinning force for oblate particles is larger than prolate particles because the matrix boundary area occluded by the oblate phase is larger (Ryum et al. 1983). Thus, pinning forces of a mineral with platy habit, such as micas, will be much larger if the migrating boundary aligns itself with the large dimensions of the plate. Likewise, deformable particles spread to occlude a larger area of the boundary and thus exert drag forces that are larger than that of a spherical particle of the same volume (see below).

As is true of unimpeded normal grain growth, even though the pinning forces are accurately known, it is much more difficult to predict the net effect of an ensemble of particles on the rate of grain growth (Nes et al. 1985). Zener's (Smith 1948) original treatment assumed that the diameter of the second-phase particles were much smaller than the matrix grains, and that the particles were randomly dispersed throughout the matrix phase. In addition to assuming that all particles are the same size and that each acts on the boundary with the maximum restraining force, Zener's treatment assumes that the boundary does not change shape as it encounters the second-phase particles. Subsequent treatments attempt to allow for various refinements in the calculations, including variable particle sizes and the changeable boundary shape (Nes et al. 1985). To first order, most models predict that the maximum grain size achieved by the matrix is

$$G_{\mathrm{max}} = C'^{(m)} \cdot \frac{d_{\mathrm{p}}}{f_{\mathrm{vol}}^{m}} \qquad (13)$$

where $C'^{(m)}$ is a constant that depends on the model assumptions (see Table 4). When the second-phase particles are small relative to the matrix and randomly dispersed throughout it, then Zener and others predict $m=1$. If the dispersion of second phase particles is non-random or if the second-phase particle size is comparable to the matrix grain size, then, for a given

Table 3 Drag force of individual particles

Particle shape Bonding	Spherical Incoherent	Spherical		Ellipsoidal	
		Coherent		Case 1 (Oblate)	Case 2 (Prolate)
Model	Smith (1948)	Gladman (1966)	Nes et al. 1985	Ryum et al. 1983	Ryum et al. 1983
Drag force	$\frac{\pi}{2}d_{\mathrm{p}}\gamma$	$1.98 \cdot d_{\mathrm{p}}\gamma$	$\pi d_{\mathrm{p}}\gamma$	$\pi d_{\mathrm{p}}\gamma\left(\frac{1}{(1+E_{\mathrm{p}})E_{\mathrm{p}}^{1/3}}\right)$	$\frac{d_{\mathrm{p}}}{2}\gamma\left(\frac{1+2.14E_{\mathrm{p}}}{E_{\mathrm{p}}^{1/2}}\right), \quad E_{\mathrm{p}} < 1$

Table 4 Limiting matrix grain size in two-phase aggregates

Equation[a]	Reference
$G_{max} = C' \cdot \frac{d}{f}$	Zener in: Smith (1948) Haroun and Budworth (1968)
$G_{max} = \left(3/2 - 2/Z\right) \cdot \left[\frac{\pi d}{6f}\right]$ where $\sqrt{2} \leq Z \leq 2$	Gladman (1966)
$G_{max} = \left[\frac{4d}{9\beta f}\right]$ where $\beta = 0.125 \cdot \ln\left(\frac{80\rho}{d}\right)$	Hellman and Hillert (1975) ρ is the boundary curvature
$G_{max} = \frac{2d}{3f} \cdot \{16/[\ln 4D_{max} \cdot (1 - 16/\ln[2D_{max}/d])]\}$	Louat (1983)
$G_{max} = C''d/f^{1/2}$	Anand and Gurland (1975) Haroun and Budworth (1968)
$G_{max} = C'''d/f^{1/3}$	Hellman and Hillert (1975)

[a] C', C'', C''' are constants, ρ is the boundary curvature, d is the diameter of the second-phase particle, f is the volume fraction of the second phase

f_{vol}, G_{max} is smaller. For example, if the particles reside solely on grain boundaries (i.e., are never included in the matrix grains), then $m=1/2$ (Haroun and Budworth 1968; Anand and Gurland 1975; Hellman and Hillert 1975). If the particles lie on grain corners only, then $m=1/3$, and G_{max} is even smaller.

Experimental determinations including computer simulations of the pinning effect also show that $G_{max} \propto f_{vol}^{-m}$ where $0.3 \leq m \leq 1.0$ (see Fig. 5) and that $G_{max} \propto d_p$ (Srolovitz et al. 1984; Olgaard and Evans 1986). In experiments of Zener pinning in hot-isostatically pressed calcite aggregates, Olgaard and Evans (1986) found that $1/3 \leq l > m \leq 1/2$, but the dependence

of G_{max} on particle size in those experiments was not systematic, owing perhaps because of particle agglomeration during the preparation of the powder compacts, or the differences in the particle size distribution functions of the second-phase powders used.

Two limiting cases seem possible, depending on the initial distribution of the second phase. On the basis of current theory and results, it seems that the Zener model [Eq. (13)] with $m=1$, provides a good estimate of the maximum grain size, provided that, initially, the second phase is randomly dispersed and that some second phase particles are included within matrix grains. Conversely, if the matrix is initially smaller than the mean free spacing of the second phase, the matrix will grow until boundaries are trapped by the second phase, then $m=1/3–1/2$. In both cases, for a fixed volume fraction, the maximum grain size is proportional to the second phase particle size.
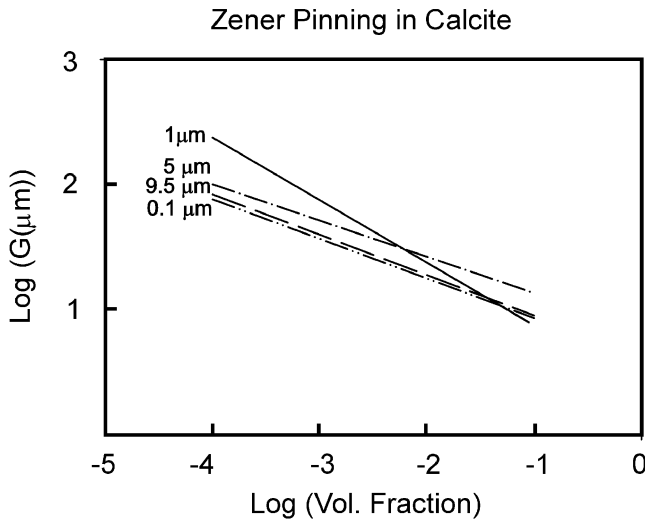
Deformable particles and pores

The same forces that result in Zener pinning may drag particles if the kinetics of transport of the components of the particle and the matrix are fast enough. For the particle to be dragged, the velocity of the boundary and the pore must be equal. The pore mobility, M_p, is defined as

$$V_p = M_p \cdot F_p \tag{14}$$

If there are N_p particles or pores on each boundary, then the net force on the boundary is the total force minus the drag forces of the particles

$$F_n = F - N_p F_p$$

Because the boundary velocity is the mobility of the boundary times the net force and because $V_p = V_b$, $V_b = M_p F_p$, and

$$V_b = M_b\left(F - \frac{N_p V_b}{M_p}\right)$$

Fig. 5 Data for Zener pinning in synthetic calcite aggregates containing second phase alumina particles with nominal particle sizes, d_p=0.1, 1, 5, and 9.5 μm (Olgaard and Evans 1986). The maximum grain size, G_{max}, is proportional to the square root or cube root of the volume fraction of second phase particles, f [(see Eq. (13)]. The samples lack a systematic relationship of G_{max} [see Eq. (13)]. to nominal particle size. The grain size relationship may be obscured because the particles are agglomerated into larger groups, or because the particle size distributions vary significantly from one set of samples to another.

Then solving for V_b,

$$V_b = F \cdot \left(\frac{M_p M_b}{M_p + N_p M_b} \right) \qquad (15)$$

When the boundary mobility is large, i.e., $N_p M_b \gg M_p$, then pore drag limits mobility, and $V_b \approx F \frac{M_p}{N_p}$. When the driving force exceeds the drag force, the particle is left behind, and the velocity is limited by the intrinsic mobility: $V_b \approx F M_b$.

Assuming for the moment that the particles are spherical and do not deform, then the maximum drag force, F_p, occurs when $\theta = 45$ [see Eq. (12)], and is $\pi \gamma d_p / 2$. The rate at which the particles can be dragged depends on the rate of transport of ions composing the matrix and the particle (Shewmon 1964). Thus the velocity of the spherical particle/pore, $V_{sph\ p}$, depends on the kinetics parameter governing transport and the dimensions of the particle/pore

$$V_{sph\ p} = C^{mech} \frac{D_0^{mech} \exp\left(-Q^{mech}/k_{BZ}T\right)}{k_{BZ}T \cdot \pi d_p^m} \cdot F \qquad (16)$$

where C^{mech}, D_0^{mech}, Q^{mech} are kinetics parameters that depend on the method of transport, e.g., surface diffusion, grain boundary diffusion, diffusion through the pore/particle; m is 2 or 3 for transport through the pore/particle, 3 for transport through the matrix lattice, and 4 if transport is limited by surface or boundary diffusion (see Table 5).

When a migrating boundary intersects a deformable particle or pore, capillary forces at the junction of the boundary and pore cause the interface to adjust its shape to form the equilibrium dihedral angle. The shapes of the particle/pore and of the boundaries surrounding it, depend on the mobility of the boundaries, the number and geometry of the boundaries intersecting the pore, the driving force exerted by the boundaries, the equilibrium dihedral angle, as well as the kinetics parameters in the simpler phenomenological equation [Eq. (16)]. Analytical and numerical solutions of the equation of motion of the particle/boundary ensemble have been obtained for several pore-boundary geometries, including two- and three-dimensional pores intersected by two or three boundary segments (Hsueh et al. 1982; Spears and Evans 1982; Svoboda and Riedel 1992; Riedel and Svoboda 1993).

In general, as the boundary force is increased, the pore will be more lenticular than spherical, and pores being dragged will have complex curvature. For the case of a two-dimensional pore, dragged by two boundary segments, and with transport limited by surface diffusion, the maximum velocity of the pore is approximately (Hsueh et al. 1982; Spears and Evans 1982)

$$V_{pore} = V_{sph\ p} \frac{17.9 - 6.2\Psi}{2 \cdot \cos(\Psi/2)} \qquad (17)$$

When the boundary forces are large (e.g., small radius of curvature), the boundary velocity may exceed the maximum pore velocity. If so, the pore is dropped from the boundary and the boundary can proceed with increased velocity. Notice that pores with large dihedral angle will be dropped at lower velocities than those with low angles.

The conditions for dragging and dropping are different for pores intersected by two boundary segments than for those intersected by three boundary segments. The drop conditions for three dimensional pores, i.e., closed, unconnected pores, intersected by two segments, are less restrictive than two-dimensional, cylindrical (i.e., connected) pores intersected by either two or three segments. Dropped porosity is often produced in experiments during the initial stages of grain growth of minerals when matrix grains are relatively small (Karato 1989a; Nichols and Mackwell 1991). By measuring the sizes of the pores that are included and those that are being dragged, one can quantitatively assess the drag/drop criterion (see Fig. 6 for an example). Unlike the three-dimensional pore, two-dimensional, connected (cylindrical) porosity shows almost no tendency towards separation, and can substantially reduce the rate of grain growth (Svoboda
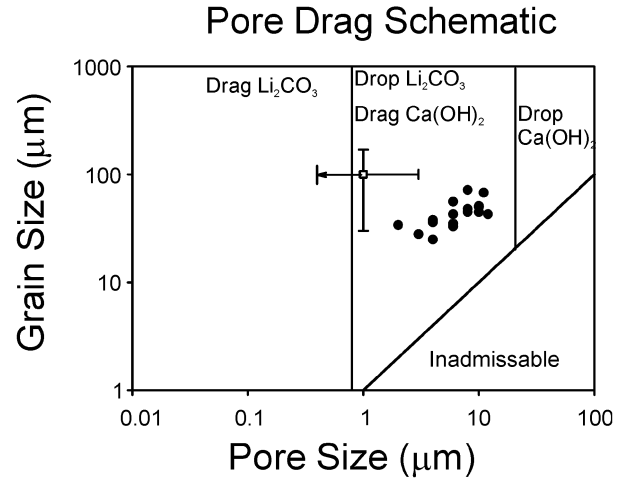

Pore Drag Schematic

Fig. 6 In partially molten carbonates, pores are dropped in the early stages of grain growth, when grain size is small and the boundaries are highly curved. By observing the sizes of pore that are being dragged or have been dropped, a drag/drop criterion can be measured. *Solid circles* are data from the melts fluxed with calcium hydroxide (low melt viscosity). The *open square* with error bars is for the system fluxed with lithium carbonate (high melt viscosity). Because pores containing low viscosity melt are more mobile, the boundary is able to drag pores of larger diameter

Table 5 Growth kinetics – pore drag (after Brook 1976)

Mechanism	n [Eq. 1.]
Surface/boundary diffusion around particle/pore	4
Lattice diffusion through the matrix	3
Transport limited by diffusion through particle/pore	3
Transport limited by interface reaction	2

and Riedel 1992). Thus, grain growth in partially molten peridotites, in which melt-filled porosity is largely connected, is slower than growth in peridotites with very low porosity (Hirth and Kohlstedt 1995). Liu and Patterson (1994a) suggest that pore mobilities may be measured by shape independent parameters determined by simple stereological measures. If true, then the determination of pore mobilities in natural geological samples might be possible.

Ostwald ripening

Capillary forces can also cause the grains in multiphase aggregates to coarsen by a process called Ostwald ripening (Lifshitz and Slyozov 1961). Such processes are important in determining texture during the early crystallization stage of igneous rocks (Park and Hanson 1999), during the coarsening of garnets (Miyazaki 1991) or, more generally, during coarsening of any porphyroblasts (Carlson 1989) in metamorphic rocks. The driving force for Ostwald ripening arises from variations in interface curvature [cf. Eq. (3), the Gibbs–Thomson or Thomson–Freundlich equation; Greenwood 1956]) that result in increased solution rates. Highly curved surfaces dissolve more quickly than flat surfaces. Consequently, small particles shrink, whereas large particles grow (Fig. 7).

The classical theory for Ostwald ripening assumes dilute concentrations and finite solubility (Greenwood 1956; Lifshitz and Slyozov 1961; Wagner 1961). The diffusion field around each precipitate is calculated with respect to a mean background value of solubility set by the free energy of material on a flat interface. The growth is uniquely described by the behavior of the average particle size, because specific, time-independent, particle-size distributions are predicted

Fig. 7 Two extreme cases for coarsening of a disperse phase. Two particles approach each other. In one case (*left-hand column*), growth occurs by encounter and subsequent intensified diffusion. In the second, growth occurs by agglomeration by physical contact and subsequent coalescence by boundary migration

(Brown 1989, 1992). The corresponding exponent, n, in Eq. (1) is 2 when the kinetics are controlled by interface reactions, and 3 when controlled by diffusion through the liquid.

For non-dilute concentrations the diffusion fields of individual precipitates overlap and the assumption that the solute concentration decays to the value of an infinite precipitate is violated. Various approximations using an elevated mean background field have been proposed: see reviews by (Voorhees and Glicksman 1984; Voorhees 1985, 1992; Jayanth and Nash 1989; Voorhees 1992). For example, Voorhees and Glicksman (1984) solve the multiple particle diffusion problem numerically and compare the results with a statistical mean field approximation. Steady-state particle-size distributions are predicted and the behavior of the average size is described by the classical growth equation with a rate constant depending on solid volume fraction.

The classical theory and the modifications towards an improved mean-field theory exclude interactions between the phases. But, once the solid phase approaches concentrations of ~50%, the assumptions in the classical theories begin to fail (Yang and German 1992). One reason is that the static picture of isolated, non-interacting phases is an oversimplification. Solid particles actually move in the liquid by Brownian motion or because of buoyancy forces (Niemi et al. 1980). The particles may interact with each other by repulsive as well as attractive forces (Shaw and Duncombe 1991). When the coarsening particles are surrounded by a solid matrix, they may be dragged during grain growth of the matrix, and undergo encounters (Yang et al. 1992).

As two solid particles of different size approach each other in a liquid, two limiting scenarios may be envisioned, depending on the relative magnitude of diffusion kinetics and particle velocities (Fig. 7). Either the smaller particle is rapidly dissolved to feed the growth of the larger particle, or physical contact between the particles is established. The first is usually called an encounter, and the second, agglomeration. Agglomeration leads to coalescence if an interface between the two particles becomes permanent (Zukas et al. 1976). The latter occurs under non-wetting conditions, i.e., the formation of a solid/solid boundary is favored over two solid/liquid interfaces. To complete the transition from an agglomerate to a single particle, the grain boundary must migrate. The grain boundary should only be able to sweep through one of the grains if the total area is continuously decreasing or if boundary anisotropy is present and the total energy of the ensemble of interfaces is lowered (Zhao et al. 1998).

Whether such characteristics as the precipitate distributions and growth exponents predicted by the classical theory remain valid when interactions become significant is a matter of debate. Most approaches modify the classical theory by introducing an
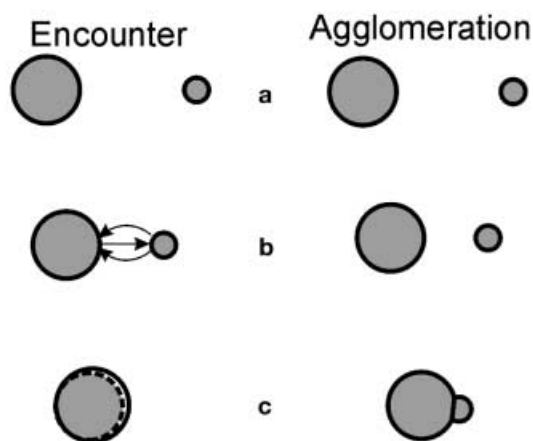
encounter integral into the continuity condition (Jayanth and Nash 1989). Using two different approaches for the case of diffusion, Brailsford and Wynblatt (1979) and Davies et al. (1979) agree that the average particle size remains proportional to the cube root of time. The grain-size distribution becomes broadened and both the distribution and the reaction constant become dependent on volume fraction. Using a statistical mechanical theory, Tokuyama et al. (1984, 1986) find two characteristic stages of coarsening, an intermediate and a late stage. During both, the average size increases with the cube root of time for diffusion-controlled coarsening [i.e., $n=3$ in Eq. (1)]. Takajo et al. (1984) used a statistical approach in which they assumed that direct coalescence is the dominant coarsening mechanism. Initially the growth kinetics indicate that $n>3$, but by the time the precipitate grains have increased by a factor of three, the size distributions approach a unique form that is considerably broader than predicted by the classical theory. In this time range, the average particle size obeys a growth law where $n=3$. Kaysser et al. (1984) found good agreement between these predictions and their experimental results. Yang and German (1992) proposed a generic grain size distribution for ~80% "precipitates" on the basis of experimentally determined grain size distributions. Recently, German and Olevsky (1998) attempted to combine Ostwald ripening and grain growth in solid materials to improve the description of the behavior of aggregates with <~50% melt. However, the complications caused by the interaction between grain boundaries and fluid-filled pores (the conditions for drag and drop) were not considered.

Discussion and conclusions

Given the apparent simplicity of the experimental protocol, the relatively large variations in kinetics observed in nominally single-phase rocks are surprising. The variations suggest that static grain growth, even in relatively simple mineralogical systems, can be affected by several parameters that are subtle, but important. Among these are porosity and pore fillings, solution impurities, boundary segregation, oxygen and water fugacity, and the presence of melt. Comparisons between studies also depend on the measurement methods.

The measurement of grain size, itself, presents a complex problem, particularly if the number distribution of size, as well as the average size, is changing or if the grain shape is anisotropic. Theories for static grain growth are predicated on the assumption that the grain size distribution normalized by the average grain size, does not change with time. Practically, measurements of the size distribution are difficult and time consuming; they are done only infrequently on planar sections, and are almost never done for all samples in a study or for three-dimensional size distributions. In fact, the time dependence of the size distribution in three dimensions may be different from that in two-dimensions (Atkinson 1988). For example, Rhines and Craig (1974) found that $\sqrt{A} \propto t^{0.43}$, whereas $\sqrt[3]{V} \propto t^{1/3}$.

Grain shape anisotropy also presents a challenge. The average intercept length, a commonly used measure for grain size, will provide a useful average measure for anisotropic grains, only if the grains are randomly oriented, or if several sectioning planes are used, and the planes are randomly oriented. In minerals, boundary energy may depend on the relative misorientation of the two bounding grains, resulting in substantial shape anisotropy. Thus, sampling may be much more difficult than in more isotropic materials. Additional complications in kinetic studies would result if the anisotropy of energy was temperature dependent.

Many minerals exist as solid-solution series, and almost all have the potential to be solvents for aliovalent ions. If segregation occurs, one might expect that solutes could exert important influences on grain boundary mobility. Covey-Crump (1997) recently suggested that solutes were responsible for the large differences in boundary migration rates in nominally pure calcite aggregates. Unfortunately, there is not enough quantitative evidence even to confirm that segregation exists. In the absence of more data it is difficult to assess the effect of impurities on grain growth. In most natural situations, many potential species will be available as solutes; additionally, these species may be buffered by stable phases, and thus be present at high fugacity. Thus, if impurity effects on grain growth are confirmed, it will be important to see if such effects saturate at high impurity content. Growth rates may also be affected by solid solutes dissolved throughout the crystal lattice, i.e., not just segregated at the boundary. Freund and Dresen (personal communication, 2000; see also Table 1) recently observed positive correlation of the rate of grain growth in hot-pressed calcite with increased manganese content. They interpreted the greater mobility as resulting from increased extrinsic diffusivity along the boundary owing to the manganese impurity.

Pore drag kinetics are also very important in determining growth kinetics in mineral systems. For example, the mobility of synthetic peridotites varies by three to four orders of magnitude depending on whether the heat-treatment is done at pressure, with or without water, with or without melt (Fig. 2). Observations of the microstructure indicate that pores are present, that they are often included within the grains during the initial stages of grain growth (i.e., dropped from the boundary) and are dragged along with the boundary during later stages of grain growth. The differences in mobility may be explained qualitatively by considering the kinetics of pore drag. At 0.1 MPa, without added water, grain growth is probably controlled by the drag of gas-filled porosity, formed dur-

ing the densification of the aggregate at higher pressure. The pore size increases during the heat -treatments because the pores containing high pressure gas expands under ambient pressure. The exact mechanism and species that limits the transport is uncertain (Nichols and Mackwell 1991). In experiments conducted at higher pressures without water, boundary mobility also increases, perhaps because the pore size remains smaller, as a result of the compression of the porous aggregate by the confining pressure. Additionally, the kinetics of transport around the pores (or through them) may be more rapid when the gas has a higher density. The stereological quantification of grain boundary–pore contacts in porous aggregates (e.g., Patterson and Liu 1990) might ultimately be used to determine relative differences in kinetic parameters determining pore or boundary mobilities in aggregates of different composition (Patterson and Liu 1990; Liu and Patterson 1994).

When melts are present, grain growth in the peridotite is faster than in samples with pores filled with low pressure gas (Cooper and Kohlstedt 1984; Karato 1989a). But, boundary migration is faster when samples are fabricated at high pressure with no added water (Hirth and Kohlstedt 1995), and are fastest when water is present (Karato 1989a). The water-added kinetics may be fast because the viscosity of the fluid phase is lower, and, therefore, diffusion kinetics are accelerated, or because added water increases lattice or boundary diffusion kinetics. It is interesting to notice that recrystallization during diffusion creep is at roughly the same speed as static grain growth (Karato 1989a). Pores and melts are ubiquitous, and, in fact, it is very difficult to find samples that do not contain one or the other or both. Thus, it is difficult to compare the mobility of melt-laden boundaries with the intrinsic mobility of a boundary with no pores or melt present. The ratio of the intrinsic mobility to the mobility of a melt film is $\delta D_l C_l / \mathrm{t} D_B$ (see Table 2 and List of symbols). There are suggestions that the ratio of the grain boundary width (without a fluid film) to the width of a melt film, i.e., δ / t, may be ~10 or less (Drury and FitzGerald 1996), in which case liquid film mobility may be comparable to or faster than the intrinsic mobility. Finally, we reiterate that there is little information on the segregation of impurities near boundaries or on the effects on boundary mobilities in this system.

To illustrate the profound effect of pores and solid second-phase on grain growth in peridotites, we show grain size versus time curves (Fig. 8) calculated using mobility data for mono-minerallic peridotites with (Nichols and Mackwell 1991) and without gas-filled porosity (Hirth and Kohlstedt 1995). The growth curves assume that the starting grain size is 1 mm, and that the temperature is 1250 °C. First, notice that grain size is from two to three orders of magnitude larger when gas-filled porosity is absent. The spread in grain size would be even larger if mobilities measured with
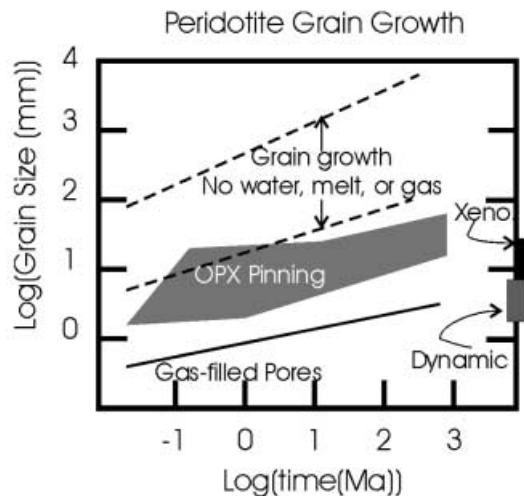

Fig. 8 Estimates for olivine grain growth at 1250 °C based on data for grain-boundary mobility. We emphasize that it is necessary to extrapolate in time by six to eight orders of magnitude. Curves are given for grain growth with no melt, water or gas porosity, for olivine grain growth controlled by Ostwald ripening of dispersed pyroxene grains, and for olivine with gas-filled porosity. Some of the kinetics parameters are known poorly, particularly for Ostwald ripening of dispersed pyroxene, so that predictions are approximate. The spread in the predictions for grain growth in the fluid and gas-absent case owes to uncertainty in the grain-size exponent in the Burke–Turnbull equation [(Eq.(1)]. For comparison, ranges in grain sizes observed for mantle xenoliths and those predicted for dynamic recrystallization are also shown. It is apparent from the data that porosity and solid second phases have profound effects on the grain growth kinetics

added water (Karato 1989a) were used. Second, notice that grains are predicted to grow much larger than typical grain sizes found, for example, in mantle xenoliths from Africa or the western North America (~4–32 mm; Ave Lallemant et al. 1980). Estimates of the grain size formed by dynamic recrystallization at strain rates thought to be appropriate to the mantle also fall within that range (van der Wal et al. 1993).

Grain size in the mantle might also be controlled by dispersed second phases. Most often the most abundant second phase is pyroxene. To estimate the effect of second-phase pinning, we assumed that the initial pyroxene grain size was between 1 and 10 mm, that the evolution of pyroxene grain size and the spacing between pyroxene grains are determined by Ostwald ripening, controlled by the diffusion of silicon along the grain boundaries in the olivine matrix phase (Farver and Yund personal communication, 2000). If the olivine matrix boundaries are pinned by the pyroxene, then the matrix grains can only grow larger as the pyroxene coarsens. With these assumptions, the predicted olivine grain size is similar to that observed in xenoliths, and is always much less than the size predicted from mobilities of boundaries unimpeded by gas bubbles. It is possible that ripening rates are actually much slower, especially if coarsening is limited by transport of Al, but it is unlikely that coarsening rates
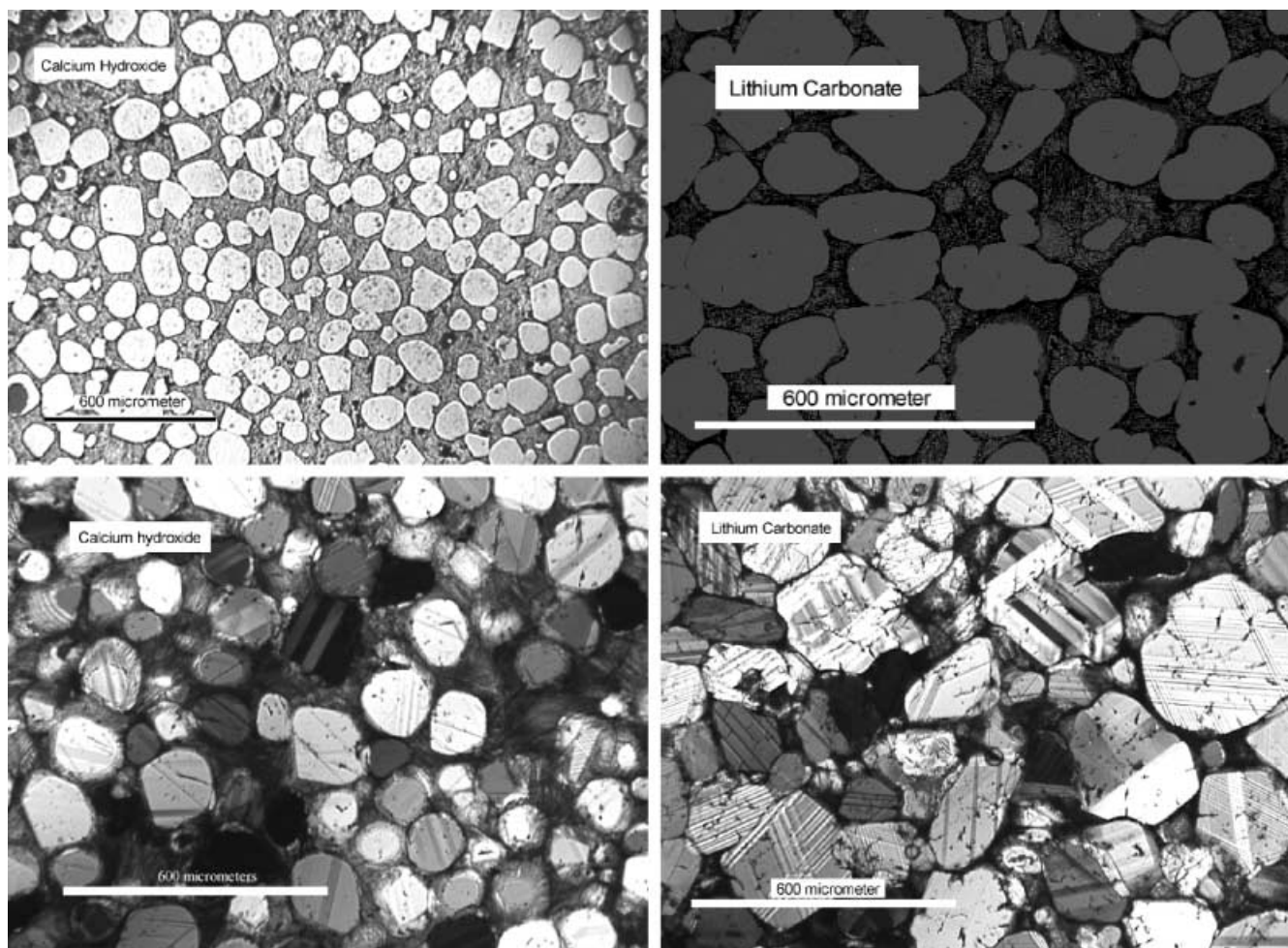
Fig. 9 Microstructures of CaCO$_3$ particles (~60% volume fraction) in eutectic melts of the systems CaCO$_3$+Ca(OH)$_2$. **a** Reflected light and **b** transmitted light with crossed polarizers. In the system CaCO$_3$+LiCO$_3$: **c** SEM. **d** Transmitted light; crossed polarizers. Aggregates were annealed at 973 K and a pressure of 300 MPa for 82.5 h. Based on the viscosity difference between the two melts, the diffusion coefficients should differ by about three to five orders of magnitude, the melt containing hydrogen being less viscous and allowing faster diffusion. Grains in the system CaCO$_3$+Ca(OH)$_2$ are equant in habit, and of a rather narrow size distribution, but have some preference for low index interfaces. Particles in the CaCO$_3$+Li$_2$CO$_3$ system have odd shapes and serrated boundaries, indicating agglomeration with subsequent coalescence. The transmitted light micrographs indicate that the particles are grain boundary free

are faster than this estimate. Thus, despite the experimental work, much uncertainty remains in our understanding of olivine growth kinetics.

Similar remarks apply to laboratory investigations of grain growth in natural and synthetic marbles. Because fine-grained aggregates are often produced by hot-pressing granular aggregates, they usually contain a small, but measurable, amount of porosity. Nearly all studies notice that pore drag affects grain growth kinetics, and pore drop often gives way to

pore drag during the course of the experiment. Kinetics in samples with no added water tend to be slower than in samples with water, (Covey-Crump 1986; Olgaard 1989), and samples with lower porosity grow fastest (Olgaard and Evans 1988). Pore capture, drag and coalescence may account for the decreasing growth kinetics often observed. If natural marbles, e.g., Solnhofen, are used, then experiments are complicated by impurities, by reactions or by dewatering of accessory minerals that often are heated above their stability fields. In experiments with water present, eutectic melting becomes possible in the temperature range 700–800 °C (Wyllie and Boettcher 1969). Thus, to predict grain growth kinetics with added water, one must understand drag of pores filled with aqueous fluids, the extent of eutectic melting and the effect of liquid film migration on growth kinetics. It is entirely plausible that impurity segregation may also affect grain growth kinetics (Covey-Crump 1986), but more information on impurity distribution is needed. Future experiments should provide detailed measurements of the pore size number distribution.

Recently, we observed agglomeration with subsequent coalescence during coarsening in the system CaCO$_3$+Li$_2$CO$_3$ (see Fig. 9). Dihedral angles between

the solid boundary and the solid/melt interfaces are ~20° so agglomerations are possible, e.g., Minarik and Watson (1995). The mechanism of the boundary migration in these particles is unclear; it seems that the agglomeration of multiple particles is required. The further development of the shape of the resulting particle is dominated by the growth of the neck left from the agglomeration (Courtney 1977a, 1977b, 1984). By contrast, when coarsening is observed in the $CaCO_3+Ca(OH)_2$ system, the encounter mechanism dominates. Although the average dihedral angles of the two systems are similar, the viscosity of the melt in the hydroxide system is from three to five orders of magnitude lower. It is interesting to notice that the absolute rates of the two systems are comparable even though the microstructure indicates that the mechanisms are different (see Fig. 9).

References

Anand L, Gurland J (1975) The relationship between the size of cementite particles and the subgrain size in quenched and tempered steels. Metall Trans 6A:928–931

Atkinson HV (1988) Overview no 65: theories of normal grain growth in pure single phase systems. Acta Metall 36:469–492

Ave Lallemant HG, Mercier J-CC, Carter NL, Ross JV (1980) Rheology of the upper mantle: inferences from peridotite xenoliths. Tectonophysics 70:85–113

Blakely JM (1973) Introduction to the properties of crystal surfaces. Pergamon Press, Oxford

Brailsford AD, Wynblatt P (1979) The dependence of Ostwald ripening kinetics on particle volume fraction. Acta Metall 27:489–497

Brook RJ (1976) Controlled grain growth. In: Wang FF-Y (ed) Ceramic fabrication procedures, vol 9. Academic Press, New York, pp 331–364

Brown LC (1989) A new examination of classical coarsening theory. Acta Metall 37:71–77

Brown LC (1992) A new examination of volume fraction effects during particle coarsening. Acta Metall Mater 40:1293–1303

Burke JE, Turnbull D (1952) Recrystallization and grain growth. Prog Metal Phys 3:220–292

Cahn JW, Balluffi RW (1981) Mechanism for diffusion induced grain boundary migration. Acta Metall 29:493–500

Carlson WD (1989) The significance of intergranular diffusion to the mechanisms and kinetics of porphyroblast crystallization. Contrib Mineral Petrol 103:1–24

Chai BHT (1974) Mass transfer of calcite during hydrothermal recrystallization. In: Hoffman BJ, Yoder HS (eds) Geochemical transport and kinetics, publication 634. Carnegie Institute of Washington, Washington, DC, pp 205–218

Chen PL, Chen IW (1996) Grain boundary mobility in Y_2O_3: defect mechanism and dopant effects. J Am Ceram 79:1801–1809

Chiang Y-M, Dunbar B, Kingery WD (1997) Physical ceramics: principles for ceramic science and engineering. Wiley, New York, pp 351–499

Cooper R, Kohlstedt DL (1984) Sintering of olivine and olivine-basalt aggregates. Phys Chem Miner 11:5–16

Courtney TH (1977a) Microstructural evolution during liquid phase sintering. Part I. Development of microstructure. Metall Trans 8A:679–684; 8A:679–684

Courtney TH (1977b) Microstructural evolution during liquid phase sintering. Part II. Microstructural coarsening. Metall Trans 8A:685–689

Courtney TH (1984) Densification and structural development in liquid phase sintering. Metall Trans 15A:1065–1074

Covey-Crump S (1986) Grain growth kinetics of calcitic aggregates. In: Geology. University of London, London

Covey-Crump SJ (1997) The normal grain growth behaviour of nominally pure calcitic aggregates. Contrib Mineral Petrol 129:239–254

Davies CKL, Nash P, Stevens RN (1979) The effect of volume fraction of precipitate on Ostwald ripening. Acta Metall 28:179–189

Drury MR, FitzGerald JD (1996) Grain boundary melt films in an experimentally deformed olivine–orthopyroxene rock: implication for melt distribution in upper mantle rocks. Geophys Res Lett 23:701–704

Drury MR, Urai JL (1990) Deformation-related recrystallization processes. Tectonophysics 172:235–253

Evans B, Hay RS, Shimizu N (1986) Diffusion-induced grain-boundary migration in calcite. Geology 14:60–63

German RM, Olevsky EA (1998) Modeling grain growth dependence on the liquid content in liquid-phase-sintered materials. Metall Mater Trans: Phys Metall Mater Sci 29A:3057–3067

Gladman T (1966) On the theory of the effect of precipitate particles on grain growth in metals. Proc R Soc Lond 294A:298–309

Greenwood GW (1956) The growth of dispersed precipitates in solutions. Acta Metall 4:243–248

Guillope M, Poirier J-P (1979) Dynamic recrystallization during creep of single-crystalline halite; an experimental study. J Geophys Res 84:5557–5567

Haroun NA, Budworth DW (1968) Modifications to the Zener formula for limitation of grain size. J Mater Sci 3:326–338

Hellman P, Hillert M (1975) On the effect of second-phase particles on grain growth. Scand J Metall 4:211–219

Hillert M (1965) On the theory of normal and abnormal grain growth. Acta Metall 13:227–238

Hirth G, Kohlstedt DL (1995) Experimental constraints on the dynamics of the partially molten upper mantle: deformation in the diffusion creep regime. J Geophys Res 100:1981–2001

Hobbs B, Means WD, Williams PF (1976) An outline of structural geology. Wiley, New York

Hsueh CH, Evans AG, Coble RL (1982) Microstructure development during final/intermediate stage sintering – I. Pore/grain boundary separation. Acta Metall 30:1269–1279

Jayanth CS, Nash P (1989) Review: factors affecting particle-coarsening kinetics and size distribution. J Mater Sci 24:3041–3052

Joesten RL (1991) Kinetics of coarsening and diffusion-controlled mineral growth. In: Kerrick DM (ed) Contact metamorphism. Mineral Soc Am, Rev Mineral 26:507–582

Karato S-I (1984) Grain-size distribution and rheology of the upper mantle. Tectonophysics 104:155–176

Karato S (1989a) Grain growth kinetics in olivine aggregates. Tectonophysics 168:255–273

Karato S (1989b) Grain-growth kinetics in olivine aggregates. Tectonophysics 168:255–273

Karato S-I, Paterson MS, FitzGerald JD (1986) Rheology of synthetic olivine aggregates: influence of grain size and water. J Geophys Res 91:8151–8176

Kaysser WA, Takajo S, Petzow G (1984) Particle growth by coalescence during liquid phase sintering of Fe–Cu. Acta Metall 32:115–122

Kohlstedt DL (1992) Structure, rheology and permeability of partially molten rocks at low melt fractions. In: Blackburn D (ed) Mantle flow and melt generation at mid-ocean ridges. Geophysical Monograph 71. American Geophysical Union, Washington, DC, pp 103–121

Lifshitz IM, Slyozov VV (1961) The kinetics of precipitation from supersaturated solid solutions. J Phys Chem Solids 19:35–50

Liu Y, Patterson BR (1994) Determination of pore mobility during sintering. Metall Mater Trans 25A:721–724

Louat N (1983) The inhibition of grain-boundary motion by a dispersion of particles. Philos Mag 47(A):907–912

Masuda T, Koike T, Yuko T, Morikawa T (1991) Discontinuous grain growth of quartz in metacherts; the influence of mica on a microstructural transition. J Metamorph Geol 9:389–402

Means WD, Park Y (1994) New experimental approach to understanding igneous texture. Geology (Boulder) 22:323–326

Minarik WG, Watson EB (1995) Interconnectivity of carbonate melt at low melt fraction. Earth Planet Sci Lett 133:423–437

Miyazaki K (1991) Ostwald ripening of garnet in high P/T metamorphic rocks. Contrib Mineral Petrol 108:118–128

Nes E, Ryum N, Hunderi O (1985) On the Zener drag. Acta Metall 33:11–22

Nichols SJ, Mackwell SJ (1991) Grain growth in porous olivine aggregates. Phys Chem Miner 18:269–278

Niemi AN, Baxa LE, Lee JK, Courtney TH (1980) Coalescence phenomena in liquid phase sintering – conditions and effects on microstructure. In: Hausner HH, Antes HW, Smith GD (eds) Modern developments in powder metallurgy, Proc 1980 Int Powder Metallurgy Conf, June 22–27, Washington, DC, vol 12. Metal Powder Industries Federation and American Powder Metallurgy Institute, Princeton, NJ, pp 483–495

Olgaard DL (1989) The role of a second phase in localizing deformation. Terra Abstr 1:377

Olgaard DL (1990) The role of second phase in localizing deformation. In: Knipe RJ, Rutter EH (eds) Deformation mechanisms, rheology, and tectonics, vol 54. Geological Society of London, London, pp 175–181

Olgaard DL, Evans B (1986) Effect of second-phase particles on grain growth in calcite. J Am Ceram Soc 69:272–277

Olgaard DL, Evans B (1988) Grain growth in synthetic marbles with added mica and water. Contrib Mineral Petrol 100:246–260

Olsson WA (1990) Grain size dependence of yield stress in marble. J Geophys Res 79:4859–4862

Park H, Ree J-H, Means WD (1997) Analogue modeling at the University at Albany, State University of New York. University at Albany, State University of New York, Albany

Park Y, Hanson B (1999) Experimental investigation of Ostwald-ripening rates of forsterite in the haplobasaltic system. J Volcanol Geotherm Res 90:103–113

Patterson BR, Liu Y (1990) Quantification of grain boundary-pore contact during sintering. J Am Ceram Soc 73:3703–3705

Powers JD, Glaeser AM (1998) Grain boundary migration in ceramics. Interface Sci 6:23–39

Rhines FN, Craig KR (1974) Mechanism of steady-state grain growth in aluminum, Metall Trans 5:413-525

Riedel H, Svoboda J (1993) A theoretical study of grain-growth in porous solids during sintering. Acta Metall Mater 41:1929–1936

Rutter EH (1984) The influence of temperature, strain rate, and interstitial water in the experimental deformation of calcite rocks. Tectonophysics 22:311–334

Ryum N, Hunderi O, Nes E (1983) On grain boundary drag from second phase particles. Scripta Metall 17:1281–1283

Schmid S, Boland JN, Paterson MS (1977) Superplastic flow in finegrained limestone. Tectonophysics 43:257–291

Shaw TM, Duncombe PR (1991) Forces between aluminum oxide grains in a silicate melt and their effect on grain boundary wetting. J Am Ceram Soc 74:2495–2505

Shewmon PG (1964) The movement of small inclusions in solids by temperature gradient. Trans Am Inst Min Metall Eng 230:1134–1137

Smith CS (1948) Grains, phases, and interfaces: an interpretation of microstructure. Trans Am Inst Min Metall Eng 175:15–51

Spears MA, Evans AG (1982) Microstructure development during final/ intermediate stage sintering. II. Grain and pore coarsening. Acta Metall 30:1281–1289

Srolovitz DJ, Anderson MP, Grest GS, Sahni PS (1984) Computer simulation of grain growth. III. Influence of a particle dispersion. Acta Metall 32:1429–1438

Stöckhert B, Duyster J (1999) Discontinuous grain growth in recrystallised vein quartz – implications for grain boundary structure, grain boundary mobility, crystallographic preferred orientation, and stress history. J Struct Geol 21:1477–1490

Sutton AP, Balluffi RW (1995) Interfaces in crystalline materials. Clarendon Press, Oxford

Svoboda J, Riedel H (1992) Pore-boundary interactions and evolution equations for the porosity and the grain size during sintering. Acta Metall Mater 40:2829–2840

Takajo S, Kaysser WA, Petzow G (1984) Analysis of particle growth by coalescence during liquid phase sintering. Acta Metall 32:107–113

Tokuyama M, Kawasaki K (1984) Statistical–mechanical theory of coarsening of spherical droplets. Physica 123A:386–411

Tokuyama M, Kawasaki K, Enomoto Y (1986) Kinetic-equations for Ostwald ripening. Physica 134(a):323–338

Tullis JA, Yund RA (1982) Grain growth kinetics of quartz and calcite aggregates. J Geol 90:301–318

Underwood EE (1970) Quantitative stereology. Addison-Wesley, Reading, MA

Urai JL, Means WD, Lister GS (1986) Dynamic recrystallization of minerals. In: Hobbs BEH, Hugh C (eds) Mineral and rock deformation: laboratory studies., The Paterson volume. Geophysics monograph 36. American Geophysical Union, Washington, DC, pp 161–200

van der Wal D, Chopra PN, Drury MR, Fitz Gerald JD (1993) Relationships between dynamically recrystallized grain size and deformation conditions in experimentally deformed olivine rocks. Geophys Res Lett 20:1479–1482

Voorhees PW (1985) The theory of Ostwald ripening. J Stat Phys 38:231–252

Voorhees PW (1992) Ostwald ripening of 2-phase mixtures. Annu Rev Mater Sci 22:197–215

Voorhees PW, Glicksman ME (1984) Ostwald ripening during liquid-phase sintering – effect of volume fraction on coarsening kinetics. Metall Trans, Phys Metall Mater Sci 15:1081–1088

Wagner C (1961) Theorie der Alterung von Niederschlägen durch Umlösen (Ostwald-reifung). Z Elektrochemie 65:581–591

Watson EB, Vicenzi EP, Rapp RP (1989) Inclusion/host relations involving accessory minerals in high-grade metamorphic and anatectic rocks. Contrib Mineral Petrol 101:220–231

Wilson CJL (1973) The prograde microfabric in a deformed quartzite sequence, Mt. Isa, Australia. Tectonophysics 19:39–81

Wyllie PJ, Boettcher AL (1969) Liquidus phase relationships in the system $CaO–CO_2–H_2O$ to 40 kilobars pressure with petrological applications. Am J Sci 267A:489–508

Yan MF, Cannon RF, Bowen HK (1977) Grain boundary migration in ceramics. In: Fulrath RM, Pask JA (eds) Ceramic microstructures, no 76. Westview Press, Boulder, pp 276–307

Yang SC, German RM (1992) Generic grain-size distribution for liquid-phase sintering. Scripta Metall Mater 26:95–98

Yang SC, Higgins GT, Nash P (1992) Coarsening kinetics of solid and liquid silver particles in nickel. Mater Sci Tech 8:10–15

Yigang X, Menzies MA, Vroon P, Mercier J-C, Chuanyong L (1998) Texture temperature geochemistry relationships in the upper mantle as revealed from spinel peridotite xenoliths from Wangquing, NE China. J Petrol 39:469–493

Zhao J, Ikuhara Y, Sakuma T (1998) Grain growth of silica-added zirconia annealed in the cubic/tetragonal two-phase region. J Am Ceram Soc 81:2087–2092

Zukas EG, Rogers PSZ, Rogers RS (1976) Spheroid growth by coalescence during liquid-phase sintering. Z Metallkd 67:591–595